ORIGINAL PAPER

Slow attractive canonical invariant manifolds for reactive systems

**Joseph M. Powers · Samuel Paolucci ·
Joshua D. Mengers · Ashraf N. Al-Khateeb**

Abstract We analyze the efficacy of a standard manifold-based reduction method used to simplify reaction dynamics and find conditions under which the reduction can succeed and fail. In the standard reduction, a heteroclinic trajectory linking saddle and sink equilibria is taken as a candidate reduced manifold which we call a Canonical Invariant Manifold (CIM). We develop and exercise analytic tools for studying the local behavior of trajectories near the CIM. In so doing, we find conditions under which nearby trajectories are attracted to the CIM (ACIM) as well as conditions for which the dynamics on the ACIM are slow (SACIM). The method is demonstrated on a (1) simple model problem, (2) Zel'dovich mechanism for nitric oxide production, and (3) hydrogen–air system. For systems that evolve in a three-dimensional composition space, we find that normal stretching away from the CIM in a volume-shrinking vector field is admitted and that depending on the magnitude of the local rotation rate, may or may not render the CIM to be attractive. The success and failure of the candidate CIM as a SACIM is displayed for the model system. Results for the Zel'dovich mechanism

J. M. Powers (✉) · S. Paolucci
Department of Aerospace and Mechanical Engineering, University of Notre Dame, Notre Dame, IN 46556, USA
e-mail: powers@nd.edu

J. D. Mengers
Office of Energy Efficiency and Renewable Energy, U.S. Department of Energy, Washington, DC, USA

A. N. Al-Khateeb
Department of Aerospace Engineering, Khalifa University, Abu Dhabi, UAE

and hydrogen–air systems are less definitive, though for specific conditions a SACIM is identified for both systems.

1 Introduction

It is widely recognized that many important physical problems possess features that can only be captured by mathematical models which are both non-linear and reflect the problems' multiscale nature. In some cases, the disparity of scales and effects of non-linearity are not severe, and a so-called direct numerical modeling approach, which employs a large number of degrees of freedom, is viable. In other cases, the disparity of scales is too large for even the most powerful computers. This necessitates the employment of additional reduction strategies in which the model is simplified in such a fashion that the essence of the solution can be captured, while reducing the required computational resources. Such reductions nearly always entail the filtering of detail. For non-linear multi-scale problems, one should ensure that such a filter has retained as much of the original nature of the full solution as possible; colloquially, one wishes to retain the "signal" and filter the "noise." However, determining what is signal and what is noise is not always straightforward.

The problem of gas-phase combustion chemistry is a paradigm example which is known both experimentally and theoretically to exhibit non-linear, multi-scale phenomena. Given the importance of combustion in practical applications, the development of both detailed models and their rational reduction has been the focus of significant effort over many decades. General background on combustion and some relevant aspects of detailed models and their reduction are summarized by Law [1].

One class of reduction which has attracted much attention in both the applied mathematics and combustion chemistry communities over the past 20 years is a so-called manifold-based method. Extensive reviews are given by Mengers and Powers [2] and Mengers [3]. Examples include works of Lam and Goussis [4], Maas and Pope [5], Roussel [6], and Büki et al. [7]. The essential idea is as follows. The dynamics of a combustion system can nearly always be modeled as an evolution of a trajectory within a finite- or infinite-dimensional phase space. For many systems, there is a rapid relaxation of a trajectory onto a manifold of lower dimension than the original space. On this lower dimensional manifold, it is often the case that only slow dynamics occur, and these are often the dynamics which are most physically relevant. If one can identify a priori such lower dimensional manifolds, it may be possible to project the trajectories of combustion dynamics onto such a manifold so that fine time scale events are "filtered," thus reducing the computational time necessary for solving a challenging and otherwise multi-scale problem. Such a manifold has been colloquially named a "slow manifold."

However, a precise definition of a slow manifold has proved non-trivial, evidence of which can be seen in a series of articles by Lorenz [8–10]; further detailed analysis
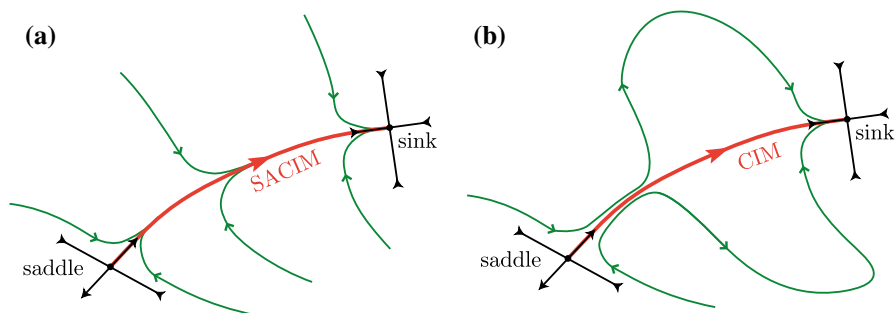
Fig. 1 Sketches of **a** one-dimensional SACIM, and **b** non-attractive CIM

for Lorenz's system was provided by Camassa and Tin [11] and Ginoux [12]. While Lorenz's questions were applied mainly to problems motivated by limit cycles for the dynamics of inert gases, they are in a general sense relevant for reactive systems which may or may not be undergoing limit cycle behavior. It is noted that a rich literature exists describing rigorous analysis of attractive manifolds, especially for inert systems undergoing limit cycle behavior, as summarized in the recent monograph of Nipp and Stoffer [13]. While studies of attractive manifolds of combustion chemistry have largely evolved independently, future studies would benefit from examining ways to provide closer linkages. That said, our approach here will be more closely aligned with the chemistry-based approach of Adrover et al. [14], who give a more detailed comparative discussion, than the non-chemistry-based approach exemplified in [13].

A visualization of a common manifold reduction introduced by Davis and Skodje [15] for combustion chemistry systems is sketched in Fig. 1a. Shown are two equilibria: one a sink which corresponds to a physical equilibrium in a closed fixed-mass combustion system [16], and the other a saddle with one unstable mode, which is a non-physical equilibrium in a combustion system. It is often possible to identify a heteroclinic connection between the saddle and the sink. Because such a connection is a trajectory, it is also an Invariant Manifold (IM) of the system, see Perko [17]. Because it is a canonical trajectory, due to its connection to the single unstable mode of the saddle, we call it a Canonical Invariant Manifold (CIM). It is well known that the CIM attracts nearby trajectories near both the saddle and sink equilibria. Figure 1a also depicts trajectories far from the equilibria that are attracted to the CIM; in combustion problems such behavior is often realized. If it is, we define the CIM to be an Attractive Canonical Invariant Manifold (ACIM). If it is further the case that relaxation to the ACIM occurs much faster than the motion on the ACIM, we call the ACIM a Slow Attractive Canonical Invariant Manifold (SACIM). Much of manifold-based reduction in combustion chemistry relies on the implicit assumption that the manifolds employed are in fact SACIMs.

Unfortunately, classical gas phase combustion models offer no guarantee that manifolds identified as a reduction have all the desirable properties found in a SACIM. Such models, which employ the law of mass action and Arrhenius kinetics, are at most guaranteed to have a unique sink equilibrium in the region of phase space where all species mass fractions are positive. Far from the sink, there is no guarantee that

trajectories nearby to the CIM are attracted to it, thus rendering the scenario of Fig. 1b a possibility. In this scenario, a trajectory which is initially near the CIM may actually be repelled from the CIM before ultimately returning to the sink equilibrium. Such a scenario would render any reduction which was based on projection onto a CIM to have large inaccuracies and would predict non-physical system behavior.

It is the purpose of this paper to describe diagnostic tools which allow one to ascertain whether a given CIM is actually a SACIM, which would have utility in rational reduction of reactive dynamics. Our main result is that CIMs need not be SACIMs, though many are, and that users of reduced chemistry should take precautions to see that any manifolds they employ do not suppress relevant chemical dynamics. We will take advantage of local linearization tools which have been previously developed, e.g. [14], for the deformation of trajectories near a CIM. These useful stretching-based diagnostics are necessary but insufficient to determine whether a CIM is a SACIM. To remedy this deficiency, we develop the notion of rotation of trajectories for three-dimensional systems and show how the competition between stretching and rotation rates can play a determining role in SACIM diagnosis. We believe the use of a rotation-based diagnostic to be novel within the reduced combustion chemistry community.

Many of these tools are similar to those employed in analyzing the kinematics of translation, stretching, and rotation of compressible fluid particles in motion, as described for example by Aris [18]. Additional general background for geometric interpretation of slow manifolds is given by Ginoux and Rossetto [19]. While some of our analysis will apply to arbitrarily large systems, most of our discussion where rotation is relevant will be limited to systems that evolve in a phase space with dimension of three. This is because the notion of a generalized rotation in higher dimensions introduces significant complications into the analysis which we will defer to future work. Indeed, realistic combustion systems are typically of higher dimension; nevertheless, we will demonstrate that even for the low dimensional systems we analyze, consideration of rotation yields new insights into chemical dynamics.

While our analysis is based on linearization near the CIM and thus will only have local validity, we note that there have been efforts made towards global analysis of manifold stability. In the context of chemical kinetic systems, one can review the global analysis of Roussel and Fraser [20], which draws upon a different strategy: functional iteration. It is intriguing that, analogous to the scenario of Fig. 1b, they note that iterations can suffer intermediate divergence from the manifold before ultimate convergence. Relevant global analysis of a different nature is considered by Ren and Pope [21], who study the evolution of trajectories emanating from a wide variety of initial conditions, including those far from a manifold of a given low dimension. They employ a local linear analysis of each trajectory, based on the singular value decomposition, to diagnose the appropriate dimension of the local slow manifold in the region far from the given manifold.

The plan of our paper is as follows. We first give a general mathematical background of CIM construction via heteroclinic connections similar to that found in [2,15], and [3]. This is accompanied by a discussion of stretching-based diagnostics similar to that of [14], as well as a new discussion of rotation-based diagnostics. We then illustrate the diagnostic tools by applying them to three problems: (1) a combustion-inspired model problem, (2) the Zel'dovich mechanism of nitric oxide production, and (3)

hydrogen–air kinetics. The first problem was originally discussed in [3]. It considers a system that evolves in a three-dimensional chemical composition space, rendering rotation to be a relevant concern. The second, the Zel'dovich model, is studied under the same conditions considered by Al-Khateeb et al. [22]. The Zel'dovich model evolves in a two-dimensional chemical composition space; thus, while stretching-based diagnostics are relevant, rotation is not. The third, the hydrogen–air model, is identical to that considered first by Ren et al. [23] and later by [22] and is restricted to a small number of species and reactions to better illustrate the geometrical features of the chemical dynamics. It evolves in a three-dimensional chemical composition space, again rendering rotation to have potential relevance. It is extracted from a larger model which describes dynamics of a more realistic hydrogen–air system. We close with brief conclusions.

2 Mathematical background

2.1 Nonlinear problem

We restrict our discussion to a spatially homogeneous ideal mixture of N ideal gases in a closed vessel with constant volume V. The constant total mixture mass is m. The number of moles of each species n_i, $i = 1, \ldots, N$, evolves in time t due to chemical reactions. We scale n_i by m to obtain the specific number of species i:

$$z_i = \frac{n_i}{m}, \qquad i = 1, \ldots, N \qquad (1)$$

At any given t only $N' \leq N$ of the z_i are linearly independent, as physical restrictions provided by principles such as element conservation for chemical reactions provide $N - N'$ linear constraints. Sometimes reaction mechanisms are such that other linear constraints exist. For example, a mechanism in which each elementary reaction has the property that the number of molecules is unchanged will have an additional linear constraint due to conservation of number of molecules. Much of the following analysis applies to $N' \geq 1$; as such, we leave N' general at this point. However, we will later confine attention to systems which have $N' = 2$ or 3, as it is those systems which best illustrate our results.

Time-dependent spatially homogeneous reaction of this mixture is described by a system of N' ordinary differential equations (ODEs) of the form

$$\frac{d\mathbf{z}}{dt} = \mathbf{f}(\mathbf{z}); \qquad \mathbf{z}(0) = \mathbf{z}_o; \qquad \{\mathbf{z}, \mathbf{z}_o, \mathbf{f}\} \in \mathbb{R}^{N'} \qquad (2)$$

Here the independent variable is t. The dependent variables z_i, $i = 1, \ldots, N'$, are embodied in $\mathbf{z}$, with $\mathbf{z}_o$ as their set of initial values. The remaining $N - N'$ values of z_i can be determined by the linear constraints. One way to develop the linear constraints is to specify a provisional set of initial conditions for z_i, $i = 1, \ldots, N$, which can later be relaxed so as to allow $\mathbf{z}_o$ to have parametric variation. The law of mass action with Arrhenius kinetics is represented within the non-linear algebraic function $\mathbf{f}$. Full details of the linear constraints and underlying physical principles are given in [2].

Equilibrium is attained at points for which

$$\mathbf{f}(\mathbf{z}) = \mathbf{0} \tag{3}$$

and in general one can expect multiple equilibria within $\mathbb{R}^{N'}$. However, it is well known, as summarized by Powers and Paolucci [16], that a unique stable equilibrium exists when $\mathbf{z}$ is restricted to values which are physically realizable. Mathematically, one can show that the eigenvalues of the Jacobian

$$\mathbf{J} = \nabla \mathbf{f} \tag{4}$$

where $\nabla = \partial / \partial z_i, i = 1, \ldots, N'$, are guaranteed real and negative at this equilibrium. The physically realizable region of $\mathbb{R}^{N'}$ is that portion for which $z_i \geq 0, i = 1, \ldots, N$, the boundary of which is a convex polytope. We define the physically realizable region as $\mathbb{S}$, its boundary as $\partial \mathbb{S}$, and the non-physical region as $\mathbb{S}'$. No species can have a negative number of moles within $\mathbb{S}$. Physical systems are further constrained by the second law of thermodynamics, which is manifested in additional restrictions on the functional form of $\mathbf{f}$. Omitting details described in [16], one can say that $\mathbf{f}$ must be constructed such that within $\mathbb{S}$, there exists a scalar function of the state variables $\mathbf{z}$ whose value changes monotonically with t through the action of $\mathbf{f}$ until it reaches an extreme value at the physical equilibrium. Depending on the particular physical scenario, that scalar function could be the entropy, the enthalpy, the Helmholtz free energy, or the Gibbs free energy. It is straightforward to formulate this scalar so that it is a Lyapunov function for the system within $\mathbb{S}$. Typically these scalar functions are singular on $\partial \mathbb{S}$.

While the state variables $\mathbf{z}$ are obviously non-physical in $\mathbb{S}'$, they are often otherwise mathematically well-behaved. In $\mathbb{S}'$, one typically finds a set of non-physical equilibria with local dynamics that can include all combinations of modes: stable, unstable, and oscillatory. For equilibria with one or more unstable modes, it is possible for there to exist a heteroclinic connection between a non-physical equilibrium and the physical equilibrium. Typically, such orbits are easy to identify by numerical integration, with values of $\mathbf{z}$ encountering no singularities (even while the second law-motivated scalar function takes on a singular value as the trajectory passes through $\partial \mathbb{S}$).

Our procedure is to focus attention on saddles with one unstable mode and to numerically integrate the system starting from a perturbation from the saddle in the eigen-direction of the unstable mode pointing towards the physical equilibrium. We call a heteroclinic trajectory connecting a non-physical equilibrium to the physical equilibrium a Canonical Invariant Manifold (CIM). Because it is often the case that a CIM is the trajectory to which the slowest dynamics of the system are confined as well as the trajectory which attracts nearby trajectories, it has the potential to be the ideal candidate for a reduced model of chemical kinetics. Because it is a trajectory, it meets well known criteria for invariant manifolds; see [17]. We focus attention on one-dimensional CIMs which originate from saddle points with one unstable mode. This guarantees that the CIM is attractive in the neighborhood of each equilibrium; far from equilibrium there is no guarantee of attraction to the CIM, as illustrated in Fig. 1b. Higher dimensional CIMs could be considered, though the topology and its

interpretation becomes more challenging. So, given a one-dimensional CIM, which is not difficult to identify, one would like to quantifiably ascertain whether such a CIM is both slow and attractive. This is more difficult, and we describe in detail in the following sections how to use a set of well-defined diagnostic tools based on linear analysis to make this determination for a general CIM.

Before proceeding to linear tools, one recognizes that a somewhat useful non-linear diagnostic tool for attractiveness of a CIM is the time evolution of the distance separating the CIM and a local trajectory which originates near the CIM as both progress towards the stable equilibrium point. We take this distance as

$$s(t) = \min_{\tau \in (-\infty, \infty)} ||\mathbf{z}_{CIM}(\tau) - \mathbf{z}(t)|| \tag{5}$$

Here $\mathbf{z}_{CIM}$ represents the CIM which is known parametrically as a function of τ. At a given time t the coordinates of a nearby trajectory $\mathbf{z}(t)$ are known, and $s(t)$ is the minimum distance from $\mathbf{z}(t)$ to any point on the entire CIM. A necessary but insufficient condition for an attractive CIM is that $s(t)/s(0) \ll 1$ as $t \to \infty$. This condition is in fact weak in that any trajectory originating within the basin of attraction of the sink equilibrium will satisfy Eq. 5. Loosely speaking, for an attractive CIM, we would like $s(t)$ for a trajectory such as that sketched in Fig. 1a to rapidly decrease to near zero on its approach to the CIM and then slowly approach zero as it moves to the sink along the CIM.

2.2 Local linear analysis

To attempt to quantify the notion of slowness and attractiveness just discussed, we will in this section pose two useful ansatzs based on local linear analysis, which will be tested a posteriori in a later section on simple examples with N' of either 2 or 3. Let us then consider Eq. 2 and require that $\mathbf{z}_o$ be a point on a CIM, far from equilibrium. Then, local linearization in the neighborhood of $\mathbf{z}_o$ gives
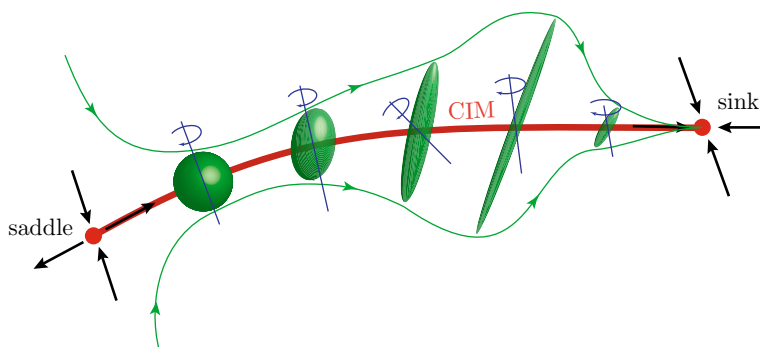
$$\frac{d}{dt}(\mathbf{z} - \mathbf{z}_o) = \mathbf{f}(\mathbf{z}_o) + \mathbf{J}|_{\mathbf{z}_o} \cdot (\mathbf{z} - \mathbf{z}_o) + \cdots . \tag{6}$$

One recognizes that $\mathbf{f}(\mathbf{z}_o)$ is a constant vector of dimension N', and $\mathbf{J}|_{\mathbf{z}_o}$ is a constant Jacobian matrix of dimension $N' \times N'$. Now let us define the symmetric and anti-symmetric parts of $\mathbf{J}$ as $\mathbf{J}_s$ and $\mathbf{J}_a$, respectively:

$$\mathbf{J}_s = \frac{\mathbf{J} + \mathbf{J}^T}{2}; \qquad \mathbf{J}_a = \frac{\mathbf{J} - \mathbf{J}^T}{2} \tag{7}$$

which allows us to recast Eq. 6 as

$$\frac{d}{dt}(\mathbf{z} - \mathbf{z}_o) = \underbrace{\mathbf{f}(\mathbf{z}_o)}_{\text{translation}} + \underbrace{\mathbf{J}_s|_{\mathbf{z}_o} \cdot (\mathbf{z} - \mathbf{z}_o)}_{\text{stretch}} + \underbrace{\mathbf{J}_a|_{\mathbf{z}_o} \cdot (\mathbf{z} - \mathbf{z}_o)}_{\text{rotation}} + \cdots . \tag{8}$$

Fig. 2 Sketch of volume and trajectory modulation near a CIM

Equation 8 describes the motion of points in the neighborhood of the CIM. For $N' = 3$, this motion has a geometric interpretation which is easily visualized. For a related detailed analysis, one can consult [21]. Because this motion is analogous to that of a three-dimensional fluid particle moving in a known velocity field, one can draw upon standard notions from differential geometry and continuum kinematics such as given in [18]; we shall draw upon many of these concepts and present results without detailed proof. As sketched in Fig. 2, one might imagine a set of points initially confined within a small sphere which is close to a non-physical saddle equilibrium point. These points evolve under the action of $\mathbf{f}$, until they are brought into the physical sink equilibrium point. Let us imagine that the volume defined by these points is monotonically shrinking with time. Mathematically, we are thus considering systems for which

$$\nabla \cdot \mathbf{f} < 0 \tag{9}$$

In the dynamical systems literature, such a system is known as dissipative. In the chemistry literature "dissipative" often has a different connotation, implying satisfaction of a second law restriction sometimes known as a Clausius–Duhem inequality. Within $\mathbb{S}$, chemistry demands the second type of dissipation, but requires the first only in the neighborhood of the physical equilibrium. As it is common for reactive systems to satisfy Eq. 9 in large portions of $\mathbb{R}^{N'}$, we will restrict discussion to systems satisfying Eq. 9 throughout. We shall see that even for such CIMs, it remains an open question as to whether they are additionally slow and attractive.

The decomposition of motion given in Eq. 8 allows one to associate $\mathbf{f}(\mathbf{z}_o)$ with translation of the volume along the CIM. The term involving $\mathbf{J}_s$ can be associated with stretching of the volume; moreover, because of the symmetry of $\mathbf{J}_s$, one can define a local orthonormal set of basis vectors as well as principal axes of stretch. The term involving $\mathbf{J}_a$ can, for $N' = 3$, be associated with rotation as a solid body about a central axis. For $N' = 3$, the dual vector associated with $\mathbf{J}_a$ is aligned with the axis of rotation, and its magnitude gives the rotation rate. For $N' > 3$, translation and stretching are not difficult to imagine, but rotation is not easily generalized.

Taking v as the small volume initially near the saddle equilibrium, one can easily show that the local relative volumetric stretching rate is given by

$$\overline{\dot{\ln v}} = \frac{1}{v}\frac{dv}{dt} = \text{tr}\,\mathbf{J} = \text{tr}\,\mathbf{J}_s = \nabla \cdot \mathbf{f} \tag{10}$$

which we consider to be negative.

Let us now select a unit vector $\boldsymbol{\alpha}$, pointing in an arbitrary direction, and use it to define a scalar σ which we associate with a local stretching rate in the direction of $\boldsymbol{\alpha}$. It is not difficult to show that

$$\sigma = \boldsymbol{\alpha}^T \cdot \mathbf{J} \cdot \boldsymbol{\alpha} = \boldsymbol{\alpha}^T \cdot \mathbf{J}_s \cdot \boldsymbol{\alpha} \tag{11}$$

Note that for any given direction $\boldsymbol{\alpha}$, the local vector of differential motion at $\mathbf{z}_o$ attributable to $\mathbf{J}_s$ is given by $\mathbf{J}_s \cdot \boldsymbol{\alpha}$. The component of $\mathbf{J}_s \cdot \boldsymbol{\alpha}$ aligned with $\boldsymbol{\alpha}$ is in fact σ. Also note that Eq. 11 gives a general result; $\boldsymbol{\alpha}$ and σ need not be an eigenvector/eigenvalue pair of either $\mathbf{J}$ or $\mathbf{J}_s$. If σ and $\boldsymbol{\alpha}$ were an eigenvalue/eigenvector pair of $\mathbf{J}_s$, they would represent an associated principal value and principal axis of stretch.

Now let us consider a CIM which is known parametrically as a function of t via numerical integration, $\mathbf{z}_{CIM}$. It is then straightforward to determine the unit tangent vector to the CIM, $\boldsymbol{\alpha}_t$, to be

$$\boldsymbol{\alpha}_t = \frac{\mathbf{f}(\mathbf{z}_{CIM})}{|\mathbf{f}(\mathbf{z}_{CIM})|} \tag{12}$$

The unit tangent is uniquely defined and points in the direction of motion; however, $\boldsymbol{\alpha}_t$ need not be a principal axis of stretch.

We next consider the unit vectors orthogonal to the direction of motion. For $N' = 1$, there can be no motion orthogonal to $\boldsymbol{\alpha}_t$. For $N' = 2$, there are two unit vectors orthogonal to $\boldsymbol{\alpha}_t$, and one can be selected. For $N' \geq 3$, there exists an infinite number of unit vectors which are orthogonal to $\boldsymbol{\alpha}_t$. Through procedures such as the Gram-Schmidt algorithm, we can select $N' - 1$ of them, labeled $\boldsymbol{\alpha}_{n,i}$, $i = 1, \ldots, N' - 1$, which are mutually orthonormal and, in combination with $\boldsymbol{\alpha}_t$, span the N'-dimensional space. Note that the $\boldsymbol{\alpha}_{n,i}$ are not unique.

With $\boldsymbol{\alpha}_t$ and $\boldsymbol{\alpha}_{n,i}$, one then has the tangential stretching rate σ_t:

$$\sigma_t = \boldsymbol{\alpha}_t^T \cdot \mathbf{J}_s \cdot \boldsymbol{\alpha}_t \tag{13}$$

and the normal stretching rates $\sigma_{n,i}$:

$$\sigma_{n,i} = \boldsymbol{\alpha}_{n,i}^T \cdot \mathbf{J}_s \cdot \boldsymbol{\alpha}_{n,i}; \quad i = 1, \ldots, N' - 1 \tag{14}$$

Because the $\boldsymbol{\alpha}_{n,i}$ are not yet uniquely determined, we have not yet determined the extreme values of $\sigma_{n,i}$, which will be of relevance.

At a generic point on a CIM, each individual stretching rate can be either positive, negative, or zero. It is also easy to show that the sum of all stretching rates yields the

relative volumetric stretching rate:

$$\overline{\dot{\ln v}} = \sigma_t + \sum_{i=1}^{N'-1} \sigma_{n,i} \tag{15}$$

and because we are focusing on systems for which volumetric stretching is negative, any positive stretching in a given direction must be more than counter-balanced by negative stretching in other directions.

2.3 Diagnostics in the normal plane

It will be useful to isolate attention to the plane whose unit normal is $\boldsymbol{\alpha}_t$. To this end, we first form the $N' \times (N' - 1)$ matrix $\mathbf{Q}_n$ whose columns are populated with the $N' - 1$ unit normals, $\boldsymbol{\alpha}_{n,i}$:

$$\mathbf{Q}_n = \begin{pmatrix} \vdots & \vdots & \vdots & \vdots \\ \boldsymbol{\alpha}_{n,1} & \boldsymbol{\alpha}_{n,2} & \vdots & \boldsymbol{\alpha}_{n,N'-1} \\ \vdots & \vdots & \vdots & \vdots \end{pmatrix} \tag{16}$$

We then project the $N' \times N'$ Jacobian $\mathbf{J}$ onto this plane to form the $(N'-1) \times (N'-1)$ Jacobian $\mathbf{J}_n$:

$$\mathbf{J}_n = \mathbf{Q}_n^T \cdot \mathbf{J} \cdot \mathbf{Q}_n \tag{17}$$

As $\mathbf{J} = \mathbf{J}_s + \mathbf{J}_a$, we also can easily show that $\mathbf{J}_n = \mathbf{J}_{ns} + \mathbf{J}_{na}$, where

$$\mathbf{J}_{ns} = \mathbf{Q}_n^T \cdot \mathbf{J}_s \cdot \mathbf{Q}_n; \qquad \mathbf{J}_{na} = \mathbf{Q}_n^T \cdot \mathbf{J}_a \cdot \mathbf{Q}_n \tag{18}$$

It is clear that $\mathbf{J}_{ns}$ is symmetric and $\mathbf{J}_{na}$ is anti-symmetric.

2.3.1 Stretching

To identify the magnitudes and directions of extremal normal stretching, one can consider $\mathbf{J}_{ns}$ and calculate its $N' - 1$ eigenvalues $\sigma_{n,i}$ and eigenvectors $\boldsymbol{\beta}_{n,i}$. Because of symmetry, these eigenvalues are purely real. It can be verified by applying a standard optimization procedure to Eq. 11, namely to select $\boldsymbol{\alpha}$ such that one extremizes $\sigma = \boldsymbol{\alpha}^T \cdot \mathbf{J}_s \cdot \boldsymbol{\alpha}$, subject to $\boldsymbol{\alpha}^T \cdot \boldsymbol{\alpha} = 1$ and $\boldsymbol{\alpha}^T \cdot \boldsymbol{\alpha}_t = 0$, that the eigenvalues of $\mathbf{J}_{ns}$ are the extreme values of σ from Eq. 11 in the plane whose unit normal vector is $\boldsymbol{\alpha}_t$. One can find the directions of extreme normal stretch via $\boldsymbol{\alpha}_{n,i} = (\mathbf{Q}_n^T)^+ \cdot \boldsymbol{\beta}_{n,i}$; here the "+" denotes the Moore–Penrose inverse. Because $\boldsymbol{\alpha}_{n,i}, i = 1, \ldots, N' - 1$, span the same space as the column vectors of $\mathbf{Q}_n$, there is no loss of information in the Moore–Penrose projection. One also has $\mathbf{Q}_n^T \cdot \boldsymbol{\alpha}_{n,i} = \boldsymbol{\beta}_{n,i}$. Direct application of the optimization procedure yields the identical directions $\boldsymbol{\alpha}_{n,i}$ associated with the extreme values of normal stretchings $\sigma_{n,i}$.

2.3.2 Rotation

We next discuss the portion of the motion in the normal plane attributable to $\mathbf{J}_a$, which for $N' = 3$ will be interpreted as being related to rotation, which is non-deforming. We first recognize that for any given direction $\boldsymbol{\alpha}$, the local vector of differential motion at $\mathbf{z}_o$ attributable to $\mathbf{J}_a$ is given by $\mathbf{J}_a \cdot \boldsymbol{\alpha}$. Part of this vector will be parallel with $\boldsymbol{\alpha}_t$, and part will be normal. The part which is normal is $\mathbf{J}_a \cdot \boldsymbol{\alpha} - (\boldsymbol{\alpha}_t^T \cdot \mathbf{J}_a \cdot \boldsymbol{\alpha})\boldsymbol{\alpha}_t$.

We then wish to identify the $\boldsymbol{\alpha}$ which is associated with the maximum magnitude of this vector in the normal plane. Thus our optimization problem is to select $\boldsymbol{\alpha}$ so as to maximize $\left|\left|\mathbf{J}_a \cdot \boldsymbol{\alpha} - (\boldsymbol{\alpha}_t^T \cdot \mathbf{J}_a \cdot \boldsymbol{\alpha})\boldsymbol{\alpha}_t\right|\right|$, subject to $\boldsymbol{\alpha}^T \cdot \boldsymbol{\alpha} = 1$, and $\boldsymbol{\alpha}^T \cdot \boldsymbol{\alpha}_t = 0$. It will be useful to take

$$||\mathbf{J}_{na}|| \equiv \omega \tag{19}$$

For $N' = 1, 2$, it is easy to show that $\left|\left|\mathbf{J}_a \cdot \boldsymbol{\alpha} - (\boldsymbol{\alpha}_t^T \cdot \mathbf{J}_a \cdot \boldsymbol{\alpha})\boldsymbol{\alpha}_t\right|\right| = ||\mathbf{J}_{na}|| = \omega = 0$ for all suitably constrained $\boldsymbol{\alpha}$. For $N' = 3$, it can be shown that *all* $\boldsymbol{\alpha}$ satisfying the constraints induce $\left|\left|\mathbf{J}_a \cdot \boldsymbol{\alpha} - (\boldsymbol{\alpha}_t^T \cdot \mathbf{J}_a \cdot \boldsymbol{\alpha})\boldsymbol{\alpha}_t\right|\right| = ||\mathbf{J}_{na}|| = \omega$. For $N' = 3$, we interpret ω as the magnitude of the relevant component of rotational velocity in the normal plane. For $N' = 3$, indeed each $\boldsymbol{\alpha}$ induces a unique vector $\mathbf{J}_a \cdot \boldsymbol{\alpha} - (\boldsymbol{\alpha}_t^T \cdot \mathbf{J}_a \cdot \boldsymbol{\alpha})\boldsymbol{\alpha}_t$; however, each of these has identical magnitude. For $N' > 3$, the value of $\left|\left|\mathbf{J}_a \cdot \boldsymbol{\alpha} - (\boldsymbol{\alpha}_t^T \cdot \mathbf{J}_a \cdot \boldsymbol{\alpha})\boldsymbol{\alpha}_t\right|\right|$ varies with suitably constrained $\boldsymbol{\alpha}$. However, its maximum value is in fact given by ω. For $N' > 3$, the geometric interpretation of ω is unclear. Equipped with these tools, we next turn to how to use them to diagnose the attractiveness and slowness of a candidate CIM.

2.3.3 Attractiveness

Loosely defined, an attractive CIM is one for which trajectories originating from points near the CIM are brought towards the CIM by the action of $\mathbf{f}$. Certainly for points on the CIM for which all possible normal stretching rates are negative: $\sigma_{n,i} < 0$; $i = 1, \ldots, N' - 1$, trajectories which originate in the near neighborhood of the CIM will be carried towards the CIM. This important result holds for all $N' > 1$. Conversely, if all possible normal stretching rates are positive, the CIM is not attractive. For $N' = 1$ there is no possibility of normal stretching, and the notion of an attractive manifold is irrelevant. If $N' = 2$, there is only one normal stretching rate, and one has sufficient information to determine attractiveness.

We next consider the interesting case where some of the $\sigma_{n,i}$ may be positive and some negative. For $N' = 3$, a CIM with one positive and one negative normal stretching rate can still be attractive in the presence of rotation in the normal plane of sufficiently large magnitude and a negative volumetric stretching rate. One can imagine a trajectory originating at a point near the CIM where $\sigma_{n,i} > 0$ for some i. Such a trajectory could be initially repelled from the CIM. However, if that trajectory is simultaneously being rotated with sufficient rapidity through the action of non-zero $\mathbf{J}_{na}$, one can imagine it being rapidly rotated out of the region of positive normal stretching into a region of negative normal stretching. If the rotation rate is sufficiently more rapid than the positive normal stretching rate, the trajectory will be modified so that it spends more time in regions of negative normal stretching than positive normal stretching, because

the overall volumetric stretching rate is negative. Thus, even though a particle could experience a small transient growth away from the CIM, it is rapidly restored by rotation to return to the CIM. Mathematically then, if for $N' = 3$, one of the extreme values of $\sigma_{n,i}$ is positive, we take as our *first ansatz* that the CIM is attractive if the ratio $\mu\ (\geq 0)$ is

$$\mu \equiv \frac{\omega}{\max_i \sigma_{n,i}} > 1; \qquad N' = 3 \tag{20}$$

This plausible hypothesis will be tested in upcoming examples. Note that μ can vary along the CIM. In practice $\mu \gtrsim 1$ may be sufficient to realize attractiveness. For $\mu \lesssim 1$ or $\mu < 1$, a trajectory could be carried far from the CIM. If the trajectory originates within $\mathbb{S}$, it will ultimately return to the physical sink. If it originates within $\mathbb{S}'$, there is no guarantee of connection to the physical sink. For systems with $N' > 3$ which have both positive and negative $\sigma_{n,i}$, it is difficult to characterize rotation, and thus difficult to arrive at a simple criteria for attractiveness.

2.3.4 Slowness

For a given attractive CIM (ACIM), we now ask if the ACIM is also slow, rendering it a SACIM. For the ACIM to be slow, one can insist that normal stretching be faster than tangential stretching on the ACIM. It is the value of $\sigma_{n,i}$ with the smallest magnitude that must be compared to the tangential stretching rate. And thus we take as a *second ansatz* that the criteria for a SACIM must be that the ACIM exist and possess

$$\kappa \equiv \frac{\min_i |\sigma_{n,i}|}{|\sigma_t|} > 1 \tag{21}$$

This too will be tested in upcoming examples. Note that κ can vary along the ACIM. Large $\kappa \gg 1$ will correspond to trajectories moving normally towards the SACIM, followed by a region of high trajectory curvature, where the trajectory then aligns to be nearly tangent to the SACIM. As $\kappa > 1$ reduces, such a trajectory will encounter weaker curvature in its relaxation to the SACIM. For $\kappa < 1$, trajectory motion will be towards the equilibrium point, but not strongly aligned with the ACIM. In practice $\kappa \gtrsim 1$ may be sufficient for a SACIM. ACIMs with $\kappa \lesssim 1$ or $\kappa < 1$ will have nearby trajectories whose dynamics are as slow or slower than those on the ACIM, thus rendering such an ACIM to be of little or no value in a rational reduction. One recognizes that any trajectory nearby an ACIM will formally coincide with the ACIM only at the sink equilibrium. A SACIM will have nearby trajectories which are rapidly pulled normally towards it, while an ACIM which is not a SACIM has nearby trajectories which evolve nearly parallel to it. We remark that a SACIM is one which locally attracts nearby trajectories to an arbitrarily close distance of the CIM on a time scale which is much faster than that of the dynamics on the CIM.

2.4 Algorithmic diagnostic procedure

We summarize an algorithmic diagnostic procedure for identification of a SACIM for a system of the form of Eq. 2 as follows:

1. Identify all equilibria by solving Eq. 3. This requires some means to solve non-linear algebraic equations.
2. Determine the Jacobian $\mathbf{J}$ from Eq. 4, along with $\mathbf{J}_s$ and $\mathbf{J}_a$ from Eq. 7.
3. Evaluate $\mathbf{J}$ near each equilibrium to determine its local dynamical character as a sink, saddle, source, etc.
4. Integrate from the neighborhood of all saddles within $\mathbb{S}'$ with one unstable mode to identify any and all heteroclinic connections to the unique sink within $\mathbb{S}$ so as to determine a one-dimensional CIM, $\mathbf{z}_{CIM}$, which is a candidate ACIM.
5. Determine the unit tangent $\boldsymbol{\alpha}_t$ along the CIM from Eq. 12.
6. Determine the tangential stretching rate σ_t along the CIM from Eq. 13.
7. Use a Gram-Schmidt procedure to identify $N'-1$ unit normal vectors, thus forming the orthonormal basis $\{\boldsymbol{\alpha}_t, \boldsymbol{\alpha}_{n,1}, \ldots, \boldsymbol{\alpha}_{n,N'-1}\}$.
8. Form $\mathbf{Q}_n$ from Eq. 16.
9. Form $\mathbf{J}_{ns}$ and $\mathbf{J}_{na}$ from Eq. 18.
10. Identify the extremal values of normal stretching and their associated directions from calculation of the eigenvalues and eigenvectors of $\mathbf{J}_{ns}$.
11. Identify ω from $||\mathbf{J}_{na}||$ and associate it with rotation for $N' = 3$.
12. If all extremal normal stretching is negative, the CIM is an ACIM; use Eq. 21 to determine κ to discern if and where the ACIM is a SACIM.
13. For $N' = 3$, if one extremal normal stretching is positive and the other negative, from Eqs. 20 and 21, determine μ and κ along the CIM so as to discern if and where the CIM is an ACIM and, moreover, a SACIM.

To concisely illustrate the system behavior, one can from Eq. 5 determine $s(t)/s(0)$ for several trajectories to demonstrate the attractiveness of the CIM.

3 Results

We present results for three problems relevant to combustion in this section. The first has a simple mathematical form and shares certain features with physically derived combustion models. It has $N' = 3$, and the magnitude of rotation will be shown to be critical in diagnosing the manifold as a CIM, ACIM, or SACIM. The second has a more complicated mathematical form, being derived from a physical combustion model. However, it has the simplifying feature of $N' = 2$, in which case rotation will be irrelevant. The third has both a physical origin as well as $N' = 3$, rendering rotation to be of potential relevance.

3.1 Combustion-inspired model problem

Let us apply these diagnostic tools to a model problem first discussed in [3]. Consider the system, of the form of Eq. 6, with $N' = 3$:

$$\frac{dz_1}{dt} = \frac{1}{20}\left(1 - z_1^2\right) \tag{22a}$$

$$\frac{dz_2}{dt} = -2z_2 - \frac{35}{16}z_3 + 2\left(1 - z_1^2\right)z_3 \tag{22b}$$

$$\frac{dz_3}{dt} = z_2 + z_3 \tag{22c}$$

The problem shares many, but not all, features with practical combustion problems. Shared features include possession of 1) non-linearity, 2) a unique stable sink equilibrium contained in the domain with positive z_i, 3) a saddle node equilibrium with not all positive z_i, 4) a heteroclinic trajectory linking the saddle to the sink, forming a CIM, 5) a local volumetric deformation rate which is strictly negative on the CIM as well as throughout the domain of positive z_i. In contrast with combustion systems, the system has no clearly identified 1) additional linear constraints, so one cannot discuss the convex polytope $\mathbb{S}$, or 2) entropy-based scalar Lyapunov function.

   This system has two finite roots, R_1 at $\mathbf{z} = (-1, 0, 0)^T$ and R_2 at $\mathbf{z} = (1, 0, 0)^T$. The Jacobian

$$\mathbf{J} = \begin{pmatrix} -\dfrac{z_1}{10} & 0 & 0 \\ -4z_1z_3 & -2 & -\dfrac{35}{16} + 2(1 - z_1^2) \\ 0 & 1 & 1 \end{pmatrix} \tag{23}$$

has eigenvalues $\boldsymbol{\lambda} = \{1/10, -1/4, -3/4\}$ at R_1 and $\boldsymbol{\lambda} = \{-1/10, -1/4, -3/4\}$ at R_2. Thus, R_1 is a saddle with one unstable mode, and R_2 is a sink, analogous to a physical equilibrium in a reactive system. There is a CIM defined by the heteroclinic orbit that connects R_1 to R_2; by inspection, it is seen that the CIM is confined to the z_1 axis with $z_1 \in [-1, 1]$ and $z_2 = z_3 = 0$. The relative volumetric stretching rate is

$$\overline{\dot{\ln v}} = \operatorname{tr} \mathbf{J} = -1 - \frac{z_1}{10} \tag{24}$$

and is negative along the entire CIM, with values ranging from $-9/10$ at R_1 monotonically decreasing to $-11/10$ at R_2. The unit tangent to the CIM is $\boldsymbol{\alpha}_t = (1, 0, 0)^T$, yielding a tangential stretching rate of

$$\sigma_t = \boldsymbol{\alpha}_t^T \cdot \mathbf{J} \cdot \boldsymbol{\alpha}_t = \begin{pmatrix} 1 & 0 & 0 \end{pmatrix} \begin{pmatrix} -\dfrac{z_1}{10} & 0 & 0 \\ -4z_1z_3 & -2 & -\dfrac{35}{16} + 2(1 - z_1^2) \\ 0 & 1 & 1 \end{pmatrix} \begin{pmatrix} 1 \\ 0 \\ 0 \end{pmatrix} = -\frac{z_1}{10} \tag{25}$$

On the CIM, we thus find that $\sigma_t \sim 1/10$ near R_1 and $\sigma_t \sim -1/10$ near the physical equilibrium R_2. On the CIM, we have

$$\mathbf{J} = \begin{pmatrix} -\dfrac{z_1}{10} & 0 & 0 \\ 0 & -2 & -\dfrac{35}{16} + 2(1 - z_1^2) \\ 0 & 1 & 1 \end{pmatrix} \tag{26}$$

and

$$
\mathbf{J}_s = \begin{pmatrix} -\dfrac{z_1}{10} & 0 & 0 \\ 0 & -2 & -\dfrac{19}{32} + 1 - z_1^2 \\ 0 & -\dfrac{19}{32} + 1 - z_1^2 & 1 \end{pmatrix} \tag{27}
$$

$$
\mathbf{J}_a = \begin{pmatrix} 0 & 0 & 0 \\ 0 & 0 & -\dfrac{51}{32} + 1 - z_1^2 \\ 0 & \dfrac{51}{32} - 1 + z_1^2 & 0 \end{pmatrix} \tag{28}
$$

A trivial Gram-Schmidt procedure yields $\boldsymbol{\alpha}_{n1} = (0, 1, 0)^T$ and $\boldsymbol{\alpha}_{n2} = (0, 0, 1)^T$, and thus

$$
\mathbf{Q}_n = \begin{pmatrix} 0 & 0 \\ 1 & 0 \\ 0 & 1 \end{pmatrix} \tag{29}
$$

The reduced Jacobian for the stretching in the normal plane is, from Eq. 18,

$$
\mathbf{J}_{ns} = \begin{pmatrix} -2 & -\frac{19}{32} + 1 - z_1^2 \\ -\frac{19}{32} + 1 - z_1^2 & 1 \end{pmatrix} \tag{30}
$$

The eigenvalues of $\mathbf{J}_{ns}$ give the extremal normal stretching rates $\sigma_{n,i}$:

$$
\sigma_{n,i} = -\frac{1}{2} \pm \frac{\sqrt{2{,}473 - 832 z_1^2 + 1{,}024 z_1^4}}{32} \tag{31}
$$

Evaluating, we find $\sigma_{n,1} \sim 1$ and $\sigma_{n,2} \sim -2$ for $z_1 \in [-1, 1]$. The presence of a positive normal stretching rate opens the possibility of divergence of a nearby trajectory from the CIM.

The reduced Jacobian for the rotation in the normal plane is, from Eq. 18,

$$
\mathbf{J}_{na} = \begin{pmatrix} 0 & -\frac{51}{32} + 1 - z_1^2 \\ \frac{51}{32} - 1 + z_1^2 & 0 \end{pmatrix} \tag{32}
$$

Its magnitude, $||\mathbf{J}_{na}|| = \omega$, on the CIM ranges from 19/32 to 51/32.

We verify that this CIM does not lead to an ACIM by direct calculation. We present the CIM and a family of trajectories which originate in the neighborhood of R_1 in Fig. 3a. The initial conditions near R_1 have $z_1 = -0.99$ and z_2, z_3 comprised of a number of equally spaced points on the circle $\sqrt{z_2^2 + z_3^2} = \epsilon = 2 \times 10^{-16}$. Clearly the trajectories remain close to the CIM at early time, but as they approach R_2, they suffer large deviations from the CIM. These large deviations are aligned with the direction of maximal normal stretching. Ultimately rotation combined with stability brings all trajectories to R_2 as $t \to \infty$. The large deviations from the CIM are consistent with the
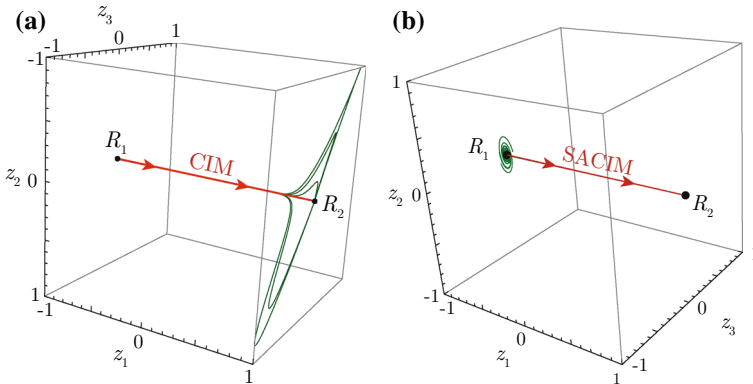
Fig. 3 Results for a simple model problem showing the heteroclinic connections and behavior of nearby trajectories for two cases: **a** weak rotation, which induces a CIM, and **b** moderate rotation, which induces a SACIM

fact that the ansatz for attractiveness, Eq. 20, is not met here. Calculation reveals that the attractiveness parameter $\mu \in [0.563, 1.43]$. Consequently there are regions where the positive normal stretching is not overcome by sufficiently rapid rotation, allowing the trajectory to suffer a large deviation from the CIM before its ultimate return to the sink at R_2. This can also be considered an effect of what is known as non-normality [24,25], a feature of dynamical systems whose Jacobians are asymmetric such as those that arise in reactive systems.

Positive normal stretching does not guarantee divergence from a CIM; it simply permits it. Since trajectories spend infinite time approaching equilibria, the time spent near a sink equilibrium in regions of negative normal stretching overwhelms the time spent in regions of positive normal stretching, which induces the ultimate return of all trajectories to the sink. However, any reduction algorithm which relies on projection onto such a CIM in regions far from equilibrium would likely induce significant error in the prediction of many state variables. Lastly, we note that nearby points to the CIM are either normally repelled or attracted much faster than motions on the CIM because the magnitude of each extremal $\sigma_{n,i}$ is much greater than σ_t. In this case, we have $\kappa \sim 5$. We easily verify the lack of attractiveness by direct calculation of $s(t)/s(0)$ from Eq. 5, which for this simple CIM is

$$
\frac{s(t)}{s(0)} = \frac{\sqrt{z_2^2(t) + z_3^2(t)}}{\epsilon}
\tag{33}
$$

Results are shown in Fig. 4a. It is seen that the relative deviation becomes large for $t \sim 100$, thus verifying that this CIM is not attractive.

If we make one minor change so as to increase the rotation rate, we find the CIM becomes a SACIM, even in the presence of regions of positive normal stretching. Let us replace Eq. 22c with

$$
\frac{dz_3}{dt} = 10z_2 + z_3
\tag{34}
$$
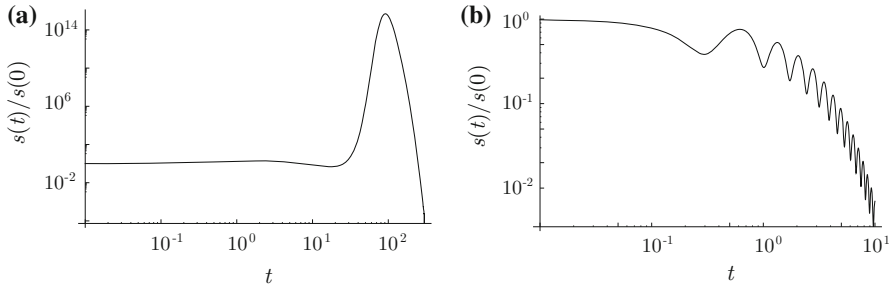
Fig. 4 Results for a simple model problem showing the evolution of the scaled distance from a nearby trajectory to the CIM: **a** weak rotation, and **b** moderate rotation

The equilibria remain the same with R_1: $(-1, 0, 0)^T$ and R_2: $(1, 0, 0)^T$. The dynamics near each equilibrium have a slight change of character. The eigenvalues of $\mathbf{J}$ near R_1 are $\lambda = \{-1/2 \pm i\sqrt{314}/4, 1/10\}$. Thus, R_1 has one linearly unstable mode and two stable oscillatory modes. The eigenvalues of $\mathbf{J}$ near R_2 are $\lambda = \{-1/2 \pm i\sqrt{314}/4, -1/10\}$. The presence of oscillatory modes near R_2 renders this model problem less like combustion problems. Nevertheless, R_2 is stable, with two of its modes containing an oscillatory character. Therefore, a CIM again exists as a heteroclinic connection between R_1 and R_2; it is confined to the z_1 axis, with $z_1 \in [-1, 1]$. The relative volumetric stretching rate is unchanged and strictly negative on the CIM, $\overline{\ln v} = -1 - z_1/10$. The tangential stretching rate on the CIM is unchanged and is $\sigma_t = -z_1/10$. The Gram-Schmidt orthogonalization is identical as well. The change induces enhanced rotation with ω ranging from $163/32$ to $195/32$. Evaluation of $\mathbf{J}_{ns}$ leads to normal stretching rates which are weakly varying functions of z_1 with extrema $\sigma_{n,1} \sim 4$ and $\sigma_{n,2} \sim -5$.

Direct calculation reveals that this modest enhancement in rotation rate is sufficient to render the CIM to be an ACIM. The ACIM is seen to be a SACIM, verifying our second ansatz, Eq. 21, as κ has a minimum value of 36.84, well above unity. We present the SACIM and a family of trajectories which originate in the near neighborhood of R_1 in Fig. 3b. The initial conditions near R_1 have $z_1 = -0.99$ and z_2, z_3 comprised of a number of equally spaced points on the circle $\sqrt{z_2^2 + z_3^2} = \epsilon = 1 \times 10^{-1}$. These were chosen further from R_1 so as to illustrate their fast attraction to the SACIM. In spite of positive normal stretching, the rotation is sufficiently fast to keep nearby trajectories close to the SACIM. Calculation reveals that the range of the attractiveness parameter on the SACIM is $\mu \in [1.10, 1.65]$. While modest, it is sufficiently large to keep the trajectories from diverging. This is verified by direct calculation of $s(t)/s(0)$ with results shown in Fig. 4b. The oscillations are attributed to the trajectory rotating in and out of regions of positive and negative $\sigma_{n,i}$.

3.2 Zel'dovich mechanism

We next consider a physically motivated problem from reaction dynamics with $N' = 2$. The Zel'dovich reaction mechanism of nitric oxide formation is adopted as used in

Table 1 Zel'dovich mechanism of nitric oxide formation [22]

j	Reaction	$A_j \left(cm^3 / \left[mol\ s\ K^{\beta_j} \right] \right)$	β_j	E_j (cal/mol)
1	$N + O_2 \rightleftharpoons NO + O$	5.841×10^9	1.01	6, 195.6
2	$N + NO \rightleftharpoons N_2 + O$	21.077×10^{12}	0.00	0.0

Sec. IV-A of [22], where more complete details of both the model and some of the analysis can be found; additional This mechanism consists of $N = 5$ species, $L = 2$ elements, and $J = 2$ reversible reactions. The kinetic data are given in Table 1.

The dependent variables are the specific moles z_i, where $i = \{1, 2, 3, 4, 5\}$ corresponds to the species $\{NO, N, O, O_2, N_2\}$, respectively. The system is taken to be isothermal and isochoric. The mixture temperature and volume are assigned as $T = 4,000$ K and $V = 10^3$ cm^3, respectively.

One can form five inhomogeneous ODEs to describe the time-evolution of the five chemical species, and one must specify an initial value for each species. At this stage, we take each of the five species to have a presence of 10^{-3} mol, though we will relax this later. As the molecular masses M_i are known to be

$$M_i = \{30.0061, 14.0067, 15.9994, 31.9988, 28.0134\} \frac{g}{mol} \qquad (35)$$

the constant mixture mass is $m = \sum_{i=1}^{5} M_i n_i = 0.120024$ g, and the constant mass density is $\rho = m/V = 1.20024 \times 10^{-4}$ g/cm^3. The initial values are

$$z_i(0) = \frac{n_i(0)}{m} = 0.00833164 \frac{mol}{g}, \qquad i = 1, \ldots, 5 \qquad (36)$$

Linear combinations of three of the ODEs can be formulated into three homogeneous ODEs, which can be integrated to form three algebraic constraints, using the initial conditions to evaluate the integration constants. Two of these constraints are due to the conservation of the elements N and O. The third is a consequence of having only bimolecular reactions, rendering the total number of moles to be time-independent. The three constraints are

$$z_1 + z_3 + 2z_4 = 0.0333266 \frac{mol}{g} \qquad (37)$$

$$z_1 + z_2 + 2z_5 = 0.0333266 \frac{mol}{g} \qquad (38)$$

$$z_1 + z_2 + z_3 + z_4 + z_5 = 0.0416582 \frac{mol}{g} \qquad (39)$$

We use these constraints to eliminate the explicit dependency of $\{O, O_2, N_2\}$ in the evolution equations for $\{NO, N\}$. Thus, we have $N' = 2$, and the system's dynamics can be fully described in the $\mathbb{R}^2$ reactive composition space, though the number of

species is 5. Because $N' = 2$, $\omega = 0$, and rotation will not play a role in the system's dynamics.

The two ODEs that describe the system's evolution are

$$\frac{dz_1}{dt} = 2.505452137 \times 10^2 + 1.161477203 \times 10^7 z_2 + 6.988326812 \times 10^8 z_2^2$$
$$- 9.976388597 \times 10^4 z_1 - 3.222205877 \times 10^9 z_2 z_1 \qquad (40)$$

$$\frac{dz_2}{dt} = 2.505452137 \times 10^2 - 1.165987934 \times 10^7 z_2 - 6.979303516 \times 10^8 z_2^2$$
$$+ 8.472811649 \times 10^4 z_1 - 1.836514615 \times 10^9 z_2 z_1 \qquad (41)$$

While we can certainly apply the initial conditions of Eq. 36, we relax these and actually choose a broader range of initial conditions for z_1 and z_2, all the while maintaining the constraints of Eqs. 37–39. This complete system, Eqs. 37–41, is identical to the one given in [22], though we include more significant digits here so that equilibria and eigenvalues can be easily independently verified. Lastly, we note that in [22], there is a small ambiguity in the definition of z_i which does not affect the results or conclusions of [22]. There, two conflicting definitions for z_i were presented. The one used in calculations in [22] as well as here is Eq. 1.

Equations 37–41 have six real isolated equilibria: three located within the finite domain, and three located at infinity. The ones located within the finite domain are:

$$R_1 \equiv \left(\mathbf{z}^e\right) = \left(-1.78 \times 10^{-5}, -1.67 \times 10^{-2}\right) \frac{\text{mol}}{\text{g}}$$

$$R_2 \equiv \left(\mathbf{z}^e\right) = \left(-4.20 \times 10^{-3}, -2.66 \times 10^{-5}\right) \frac{\text{mol}}{\text{g}}$$

$$R_3 \equiv \left(\mathbf{z}^e\right) = \left(3.05 \times 10^{-3}, 2.94 \times 10^{-5}\right) \frac{\text{mol}}{\text{g}}$$

Here, R_1 and R_2 are non-physical equilibria, while R_3 is a physical root that corresponds to the reactive system's unique physical equilibrium. Linear analysis within the neighborhood of each finite critical point reveals that R_3 is a sink, R_1 is a source, and R_2 is a saddle. The eigenvalue spectrum associated with each finite critical point is

$$R_1 : (\boldsymbol{\lambda}) = \left(4.18 \times 10^7, 2.35 \times 10^7\right) \text{ s}^{-1}$$

$$R_2 : (\boldsymbol{\lambda}) = \left(-4.64 \times 10^6, 7.11 \times 10^5\right) \text{ s}^{-1}$$

$$R_3 : (\boldsymbol{\lambda}) = \left(-1.73 \times 10^7, -1.91 \times 10^5\right) \text{ s}^{-1}$$

The system's temporal stiffness, defined as the ratio between the largest (slowest) and the smallest (fastest) time scales at the physical equilibrium point, is 90.58.

The three equilibria located at infinity are identified using the projective space technique described in [22]. The Zel'dovich system in the projective space is realized

by the following transformation: $Z_1 = 1/z_1$, $Z_2 = z_2/z_1$. The equilibria are:

$$I_1 \equiv (\mathbf{Z}^e) = (0, 0)$$
$$I_2 \equiv (\mathbf{Z}^e) = (0, 1.01)$$
$$I_3 \equiv (\mathbf{Z}^e) = (0, 2.60)$$

Analysis within the neighborhood of each critical point reveals that I_2 is a source, I_3 is a saddle, and I_1 is a saddle-node. Note that I_1 is a non-hyperbolic critical point, so the Hartman–Grobman theorem is not applicable. Instead the normal form theory is utilized to find that I_1 is a saddle-node, which consists of two hyperbolic sectors, one parabolic sector, and three separatrices. Only one of these separatrices is unstable.

The eigenvalue spectrum associated with each finite critical point is

$$I_1 : (\lambda) = \left(-1.84 \times 10^9, 0\right) \frac{g}{mol\ s^2}$$
$$I_2 : (\lambda) = \left(2.54 \times 10^9, 1.12 \times 10^9\right) \frac{g}{mol\ s^2}$$
$$I_3 : (\lambda) = \left(3.65 \times 10^9, -2.90 \times 10^9\right) \frac{g}{mol\ s^2}$$

Following the procedure presented in [22], the system's three saddles are the candidate points, and they are categorized based on their location. The first category contains the finite candidate point, and the second one contains the candidate points located at infinity ordered based on the magnitude of their positive eigenvalue. Within each category the first candidate point is the one with the least positive eigenvalue among the candidate points. So, the first candidate point is R_2, the second one is I_1, and the last one is I_3. Then, two canonical invariant manifolds (CIMs), i.e. heteroclinic orbits, are generated from the first two candidates via integrating the dynamical system starting from R_2 and I_1 in the direction of the eigenvectors associated with the candidate points' positive eigenvalues pointing towards the reactive system's physical equilibrium, R_3. The generated two CIMs presented in Fig. 5 are connected with R_3 along its slowest mode. The attractiveness of these two CIMs is clearly shown in Fig. 5; they are attracting all the trajectories inside the physically accessible domain. These results are identical to the ones presented in [22]. The species evolution along the two CIMs is presented in Fig. 6, where in Fig. 6b the species evolution is illustrated in the original reactive composition space by mapping back the obtained results in the projective space via employing the following transformation: $z_1 = 1/Z_1$, $z_2 = Z_2/Z_1$. All species have $z_i > 0$ within $\partial\mathbb{S}$. Moreover, both approach the same equilibrium R_3, though that is difficult to discern in Fig. 6 due to the scaling.

To investigate the attractiveness and slowness of the two constructed CIMs, stretching-based diagnostics are employed locally along the CIMs. The local relative volumetric deformation rate of the systems along both CIMs is presented in Fig. 7. The relative volumetric deformation rates are negative. The tangential stretching rates along the two CIMs are presented in Fig. 8. Along R_2 to R_3, σ_t is initially positive, but then becomes negative as it approaches the physical equilibrium. Along I_1 to R_3, σ_t is always negative. Figure 9 gives the single normal stretching rate and shows that both
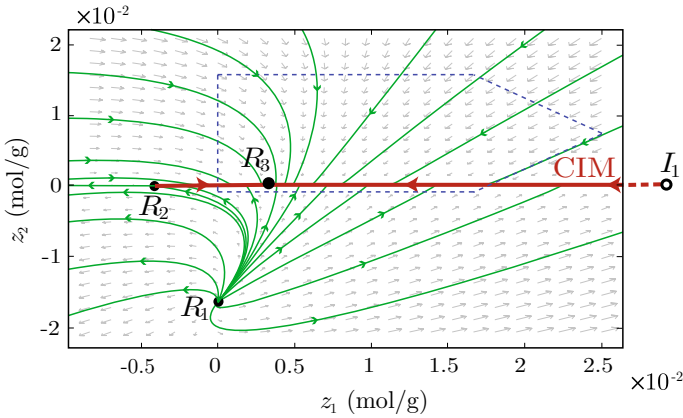
Fig. 5 The two CIMs for the Zel'dovich system illustrated as *thick lines*. The *solid dots* are finite critical points, and the *circles* are *critical points* located at infinity; R_3 represents the system's physical equilibrium state, R_2 represents starting point of the first CIM, and I_1 represents the starting point of the second CIM. The *dashed simplex* represents the boundary $\partial\mathbb{S}$ of the physical domain, and the *thin green lines* illustrate several trajectories with the *arrows* indicating motion for increasing t (Color figure online)
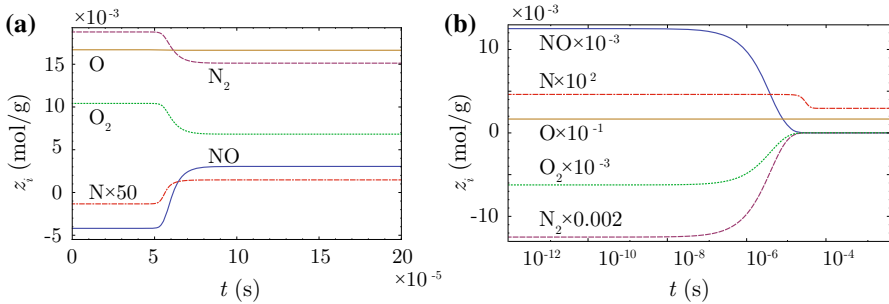
Fig. 6 The time evolution of species along the **a** $R_2 \rightarrow R_3$ and **b** $I_1 \rightarrow R_3$ CIMs for the Zel'dovich system

CIMs, $R_2 \rightarrow R_3$ and $I_1 \rightarrow R_3$ are attractive because σ_n along the CIMs is always negative. Thus, the two constructed CIMs are ACIMs. For this $N' = 2$ system, rotation is irrelevant. Figure 10 confirms our second ansatz and shows that the dynamics on the two ACIMs are slow, because κ along the two ACIMs is greater than unity. This indicates that the motion on the two ACIMs is slower than the motion onto the ACIMs. So, these two ACIMs are SACIMs. One must recognize that we have only studied a single case and that it is possible that other conditions exist for which the CIMs are not SACIMs.

3.3 Hydrogen–air combustion

We next consider a more complicated system with $N' = 3$ for which rotation could be relevant. We examine the physically motivated combustion problem given first by
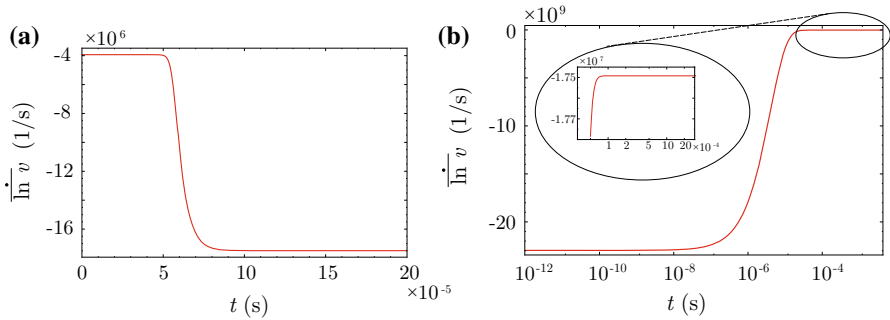
Fig. 7 The relative volumetric deformation rate along the **a** $R_2 \rightarrow R_3$ and **b** $I_1 \rightarrow R_3$ CIMs for the Zel'dovich system
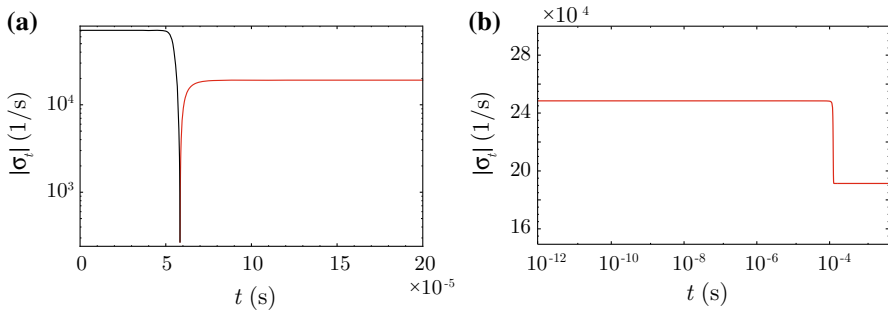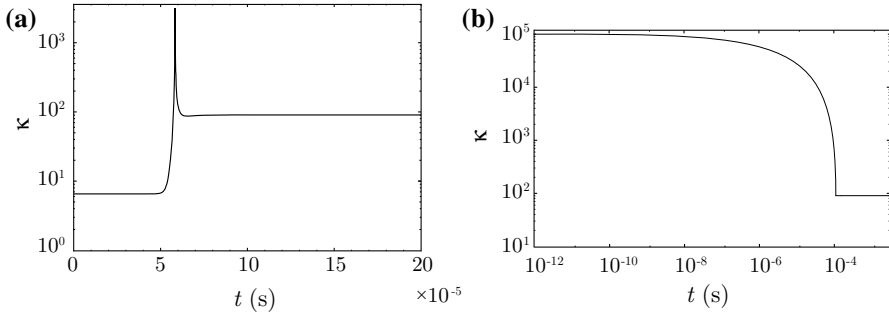

Fig. 8 The tangential stretching rate along the **a** $R_2 \rightarrow R_3$, **b** $I_1 \rightarrow R_3$ CIMs for the Zel'dovich system. The *red color* indicates negative value and the *black color* indicates positive value; the *spike* indicates switching signs (Color figure online)
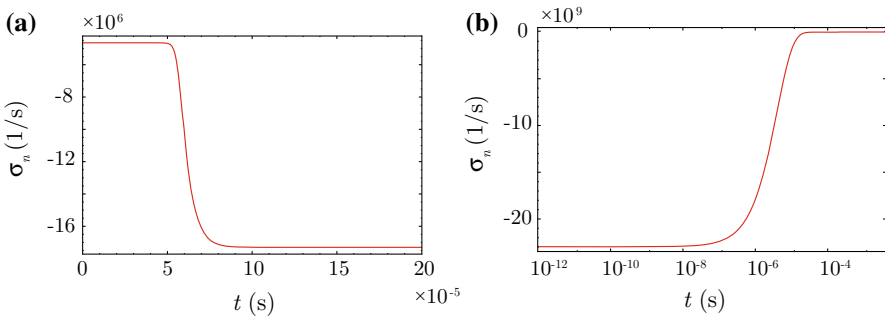
Fig. 9 The normal stretching rate along the **a** $R_2 \rightarrow R_3$, **b** $I_1 \rightarrow R_3$ CIMs for the Zel'dovich system

[23] and later studied by [22], each of whom provide more extensive details. The reaction mechanism contains $N = 6$ species, $L = 3$ elements, and $J = 6$ reversible reactions; see Table 2. The dependent variables are the specific moles $z_i = n_i/m$, $i = \{1, 2, 3, 4, 5, 6\}$ and correspond to the species {H_2, O, H_2O, H, OH, N_2}, respectively. As is standard in reaction dynamics, M represents a generic third body. The system

(a)

(b)

Fig. 10 The ratio of the normal and tangential stretching rates along the **a** $R_2 \rightarrow R_3$, **b** $I_1 \rightarrow R_3$ CIMs for the Zel'dovich system

Table 2 Simplified hydrogen–air mechanism of [23]

j	Reaction	$A_j \left[cm^3 / \left(mol\ s\ K^{\beta_j} \right) \right]$	β_j	E_j (cal/mol)
1	$O + H_2 \rightleftharpoons H + OH$	5.08×10^4	2.7	6,290.0
2	$H_2 + OH \rightleftharpoons H_2O + H$	2.16×10^8	1.5	3,430.0
3	$O + H_2O \rightleftharpoons 2OH$	2.97×10^6	2.0	13,400.0
4	$H_2 + M \rightleftharpoons 2H + M$	4.58×10^{19}	-1.4	104,380.0
5	$O + H + M \rightleftharpoons OH + M$	4.71×10^{18}	-1.0	0.0
6	$H + OH + M \rightleftharpoons H_2O + M$	3.80×10^{22}	-2.0	0.0

The non-unity third body collision efficiency coefficients are: $\alpha_{j,H_2} = 2.5$, $\alpha_{j,H_2O} = 12$, $j = 4, 5, 6$.

under consideration is isothermal and isobaric. The mixture temperature and pressure are $T = 3,000$ K and $p = 1$ atm, respectively.

One can form $N = 6$ ODEs to describe the time-evolution of the six species, and one must specify an initial value for each species. Because of element conservation, three of the ODEs have first integrals, yielding three algebraic constraints and three ODEs. Because reactions 4–6 do not conserve molecules, there is no constraint associated with the number of molecules. The three ODEs that describe the system's temporal evolution are of the form of Eq. 2 with $N' = N - L = 3$. Because they are lengthy, they are not given here. Thus, the dynamics are fully described by evolution equations for $\{H_2, O, H_2O\}$, and the rest of the species, $\{H, OH, N_2\}$, are given by the $L = 3$ linear constraints:

$$2z_1 + 2z_3 + z_4 + z_5 = 1.234 \times 10^{-2} \frac{mol}{g} \tag{42}$$

$$z_2 + z_3 + z_5 = 4.11 \times 10^{-3} \frac{mol}{g} \tag{43}$$

$$2z_6 = 6.581 \times 10^{-2} \frac{mol}{g} \tag{44}$$

which are identical to those given in [22,23]. These are easily solved to give z_4 and z_5 as functions of z_1, z_2, and z_3. Because N_2 is modeled as inert, z_6 remains constant. As for the Zel'dovich system, we actually study a variety of initial conditions for z_1, z_2, and z_3, all the while maintaining the constraints of Eqs. 42–44.

As discussed in [22], the system has fifteen equilibrium points located within the finite domain; eight of them are complex, and seven are real. The real ones are

$$R_1 \equiv (\mathbf{z}^e) = \left(-1.67204 \times 10^{-1}, 3.03617 \times 10^{-3}, 3.53209 \times 10^{-3}\right) \frac{\text{mol}}{\text{g}}$$

$$R_2 \equiv (\mathbf{z}^e) = \left(6.44204 \times 10^{-2}, 1.20566 \times 10^{-2}, -7.12337 \times 10^{-3}\right) \frac{\text{mol}}{\text{g}}$$

$$R_3 \equiv (\mathbf{z}^e) = \left(-6.47244 \times 10^{-3}, -2.00868 \times 10^{-2}, -2.19220 \times 10^{-3}\right) \frac{\text{mol}}{\text{g}}$$

$$R_4 \equiv (\mathbf{z}^e) = \left(1.97888 \times 10^{-3}, 5.03888 \times 10^{-3}, 9.41881 \times 10^{-3}\right) \frac{\text{mol}}{\text{g}}$$

$$R_5 \equiv (\mathbf{z}^e) = \left(-1.21290 \times 10^{-3}, -4.44837 \times 10^{-3}, 5.03482 \times 10^{-3}\right) \frac{\text{mol}}{\text{g}}$$

$$R_6 \equiv (\mathbf{z}^e) = \left(2.72293 \times 10^{-3}, 3.34454 \times 10^{-4}, 4.71857 \times 10^{-3}\right) \frac{\text{mol}}{\text{g}}$$

$$R_7 \equiv (\mathbf{z}^e) = \left(2.02552 \times 10^{-3}, 3.10118 \times 10^{-4}, 3.06770 \times 10^{-3}\right) \frac{\text{mol}}{\text{g}}$$

Note that R_4 and R_6 are in $\mathbb{S}'$ because other species specific mole numbers obtained from the linear constraints are negative. Thus, R_7 is the unique physical equilibrium in $\mathbb{S}$, as indicated in Fig. 11, where the dashed simplex outlines the convex polytope forming $\partial\mathbb{S}$. Also, the system has two higher dimensional equilibria located at infinity. One is one-dimensional and the other two-dimensional.

Linear analysis in the neighborhood of each real, finite critical point reveals that R_3 and R_7 are sinks, and R_1, R_2, R_4, R_5, and R_6 are saddles. The eigenvalue spectrum associated with each finite critical point is

$$R_1 : (\lambda) = \left(2.92 \times 10^3, -6.67 \times 10^6 \pm i1.00 \times 10^8\right) \text{ s}^{-1}$$

$$R_2 : (\lambda) = \left(1.84 \times 10^{14}, -1.27 \times 10^{12}, -1.70 \times 10^{14}\right) \text{ s}^{-1}$$

$$R_3 : (\lambda) = \left(-1.03 \times 10^5, -2.97 \times 10^7 \pm i2.64 \times 10^7\right) \text{ s}^{-1}$$

$$R_4 : (\lambda) = \left(1.62 \times 10^7, 8.94 \times 10^6, -4.65 \times 10^4\right) \text{ s}^{-1}$$

$$R_5 : (\lambda) = \left(3.22 \times 10^4, -2.13 \times 10^6 \pm i6.71 \times 10^6\right) \text{ s}^{-1}$$

$$R_6 : (\lambda) = \left(1.57 \times 10^4, -6.28 \times 10^6 \pm i4.37 \times 10^6\right) \text{ s}^{-1}$$

$$R_7 : (\lambda) = \left(-5.59 \times 10^3, -9.08 \times 10^6, -1.77 \times 10^7\right) \text{ s}^{-1}$$
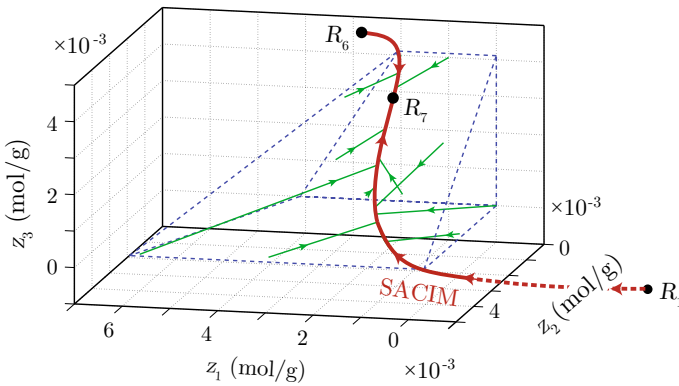
Fig. 11 Two CIMs, $R_1 \rightarrow R_7$ and $R_6 \rightarrow R_7$, for the simple hydrogen–air reactive system illustrated as *thick lines*. The *solid dots* are finite critical points; R_7 represents the system's physical equilibrium state, R_1 represents starting point of the first CIM, and R_6 represents the starting point of the second CIM. The *dashed simplex outlines* the convex polytope defining $\partial \mathbb{S}$, and the *thin lines* illustrate several trajectories. The variables z_1, z_2, and z_3 are associated with H_2, O, and $H_2 O$, respectively

Using our earlier definition, the system's temporal stiffness is 3166. Out of the seven real finite zero-dimensional equilibria, there is one sink, R_7, located in $\mathbb{S}$, one sink, R_3, located in $\mathbb{S}'$, and four saddles with one unstable mode: R_1, R_2, R_5, and R_6, all in $\mathbb{S}'$. The root R_4 has two unstable modes.

Following the procedure presented in [22], these four saddles are candidate points for the one-dimensional CIM, and they are ordered based on the magnitude of their positive eigenvalue; the first candidate point is the one with the least positive eigenvalue among all candidate points. So, the first candidate point is R_1, the second one is R_6, the third one is R_5, and the last one is R_2. Then, two CIMs are generated from the first two candidates via integrating the dynamical system starting from R_1 and R_6 in the direction of the eigenvectors associated with the candidate points' positive eigenvalues pointing towards the reactive system's physical equilibrium, R_7. These two CIMs, presented in Fig. 11, connect with R_7 along its slowest mode. The attractiveness of these two CIMs is shown in Fig. 11; they are attractive to other trajectories within the physically accessible domain, $\mathbb{S}$. The species evolution along the two CIMs is presented in Fig. 12. The other two candidate points, R_5 and R_2, generate another two CIMs that connect with the unphysical sink R_3 as depicted in Fig. 13.

To quantify the attractiveness and slowness of the physically relevant CIMs, $R_1 \rightarrow R_7$ and $R_6 \rightarrow R_7$, stretching-based diagnostics are employed locally along the CIMs. The local relative volumetric deformation rate of the systems is presented in Fig. 14. The relative volumetric deformation rates are negative. The local rotation and tangential stretching rates along the two CIMs are presented in Figs. 15 and 16, respectively. The tangential stretching rates undergo sign changes, indicated by a change in color in Fig. 16.

Figure 17 shows that the $R_1 \rightarrow R_7$ CIM may not be attractive because one of the extremal normal stretching rates $\sigma_{n,i}$ along the CIM is positive. However, Fig. 18 indicates that the repulsion is overcome by the local rotation rate along the $R_1 \rightarrow R_7$
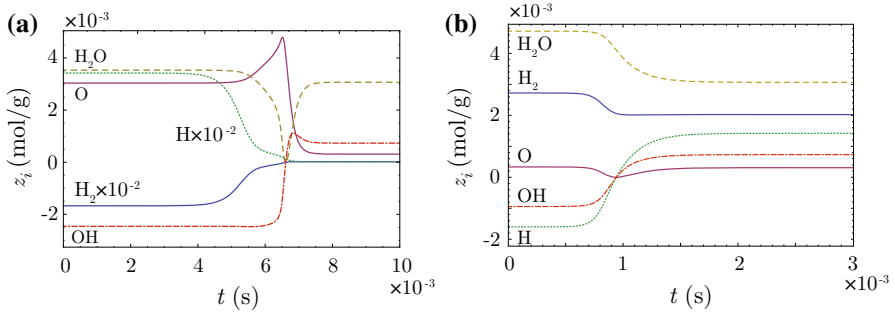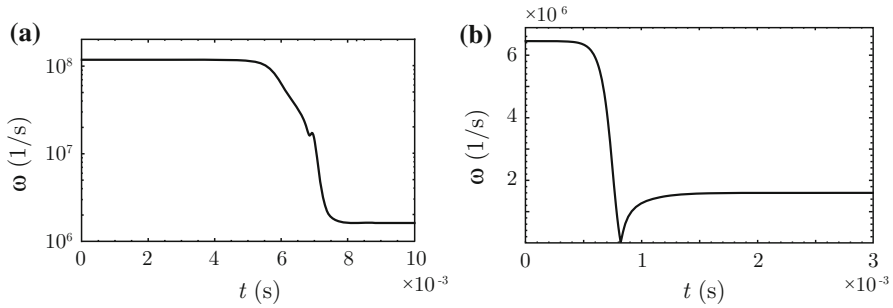
Fig. 12 The time evolution of species along the **a** $R_1 \rightarrow R_7$ and **b** $R_6 \rightarrow R_7$ CIMs for the simple hydrogen–air system
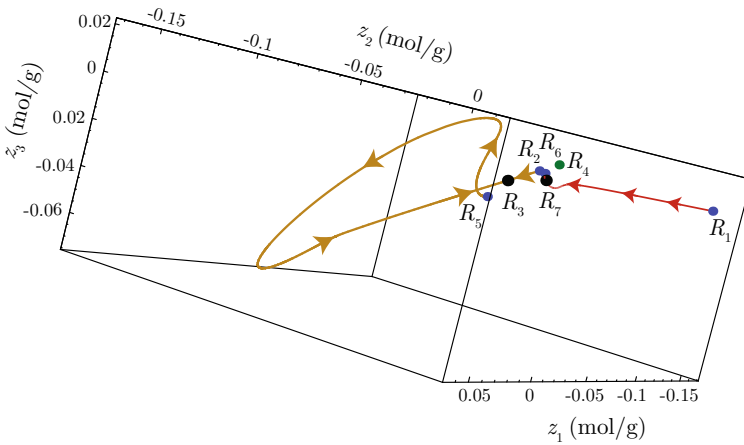

Fig. 13 Phase space for simple hydrogen–air dynamics. The *black dots* are the dynamical system's sinks, the *blue dots* are the candidate points, the *green dot* is a saddle with two unstable modes, the *red line* represents the two CIMs that connect R_1 and R_6 with the physical sink R_7, and the *gold line* illustrates the two CIMs that connect R_5 and R_2 with the unphysical sink R_3 (Color figure online)
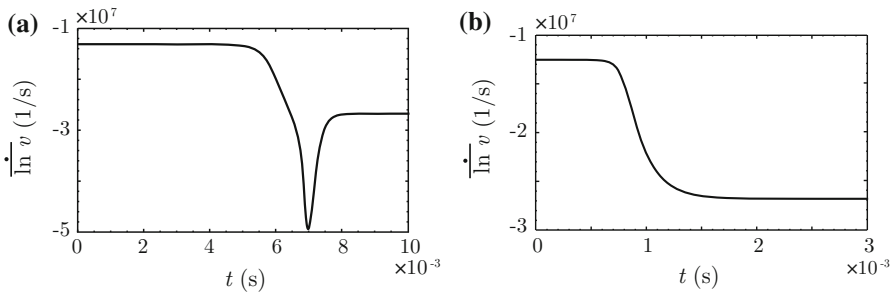
Fig. 14 The relative volumetric deformation rate along the **a** $R_1 \rightarrow R_7$ and **b** $R_6 \rightarrow R_7$ CIMs for the simple hydrogen–air system
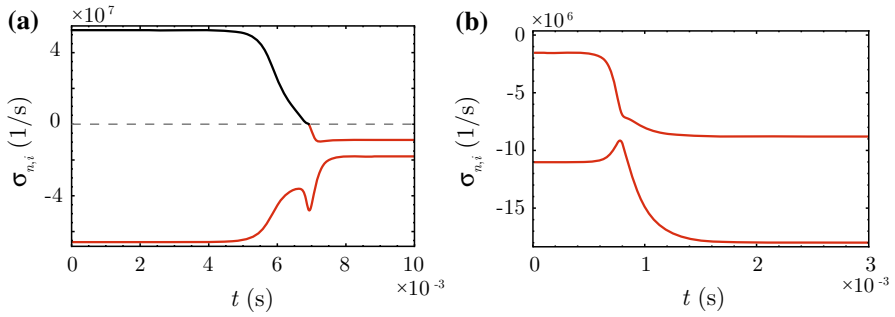
Fig. 15 The local rotation rates along the **a** $R_1 \rightarrow R_7$ and **b** $R_6 \rightarrow R_7$ CIMs for the simple hydrogen–air system
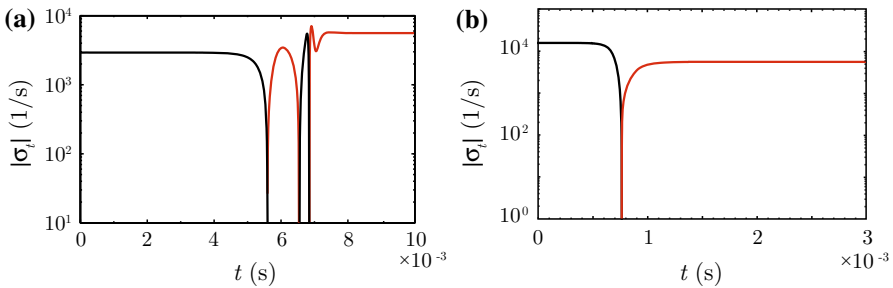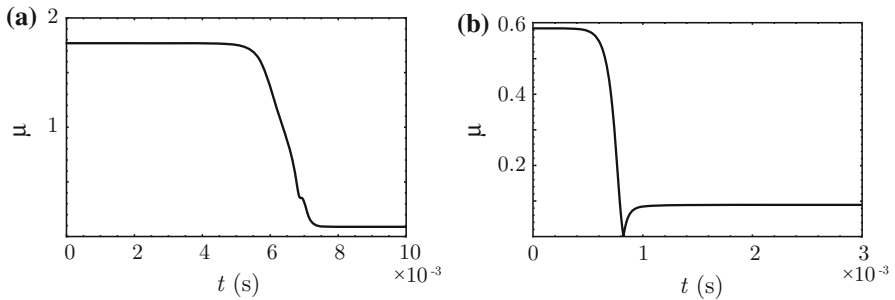

Fig. 16 The tangential stretching rates along the **a** $R_1 \rightarrow R_7$ and **b** $R_6 \rightarrow R_7$ CIMs for the simple hydrogen–air system. The *red color* indicates negative value and the *black color* indicates positive value; the *spike* indicates switching signs (Color figure online)

CIM, because μ along the $R_1 \rightarrow R_7$ CIM is greater than unity in the section of the CIM where repulsion exists; the rotation is sufficiently fast to prevent any trajectories from diverging from the CIM. Indeed at late time $\mu < 1$; however, simultaneously all $\sigma_{n,i} < 0$, rendering the rotation irrelevant at late time. Thus, the two CIMs are ACIMs. This is confirmed by plotting several trajectories originating near both CIMs, where the results are presented in Fig. 19. It is shown that both CIMs are attractive. The rotational effect has a major influence along the $R_1 \rightarrow R_7$ CIM, suppressing the effect of positive normal stretching. For the $R_6 \rightarrow R_7$ CIM, the rotation is weak; however, the normal stretching is strictly negative, thus rendering the CIM attractive.

Figure 20 indicates that the dynamics on the constructed two ACIMs are slow, because κ along the two ACIMs is greater than unity. This suggests that the motion on the two ACIMs is slower than the motion onto the two ACIMs; i.e. these two ACIMs are SACIMs. Finally, in Fig. 21, we show the physically relevant SACIMs as they evolve in both the physical $\mathbb{S}$ and non-physical $\mathbb{S}'$. The SACIMs here are colored by the magnitude of the relative slowness κ. Clearly within $\mathbb{S}$ where $\kappa \sim 10^3$, the one-dimensional manifold captures the slow dynamics of the system.
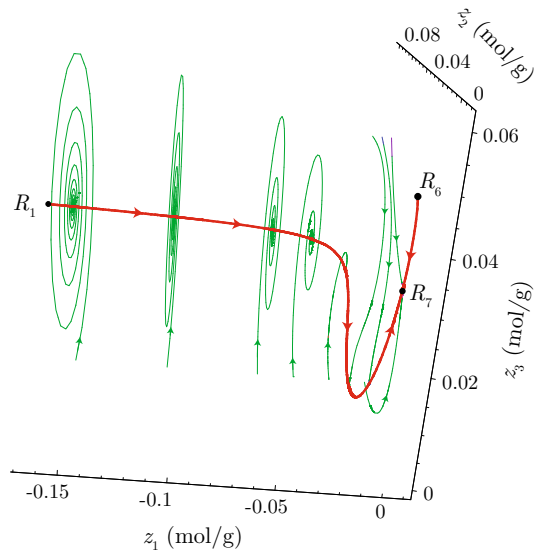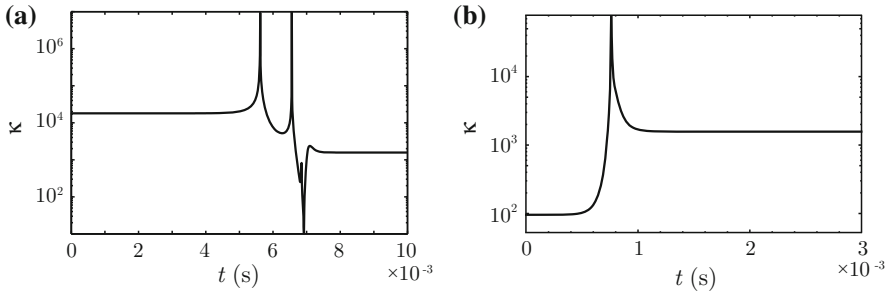
Fig. 17 The normal stretching rates along the **a** $R_1 \rightarrow R_7$ and **b** $R_6 \rightarrow R_7$ CIMs for the simple hydrogen–air system. The *red color* indicates negative value and the *black color* indicates positive value (Color figure online)


Fig. 18 The time evolution of the ratio of rotation to normal maximum stretching rates $\mu(t)$ along the **a** $R_1 \rightarrow R_7$ and **b** $R_6 \rightarrow R_7$ CIMs for the simple hydrogen–air system

Fig. 19 Illustration exhibiting how the SACIMs for the simple hydrogen–air system attract nearby trajectories for both $R_1 \rightarrow R_7$ and $R_6 \rightarrow R_7$

Fig. 20 The time evolution of the ratio of minimum normal stretching rate to the tangential stretching rate, $\kappa(t)$, along the a) $R_1 \to R_7$ and b) $R_6 \to R_7$ CIMs for the simple hydrogen–air system. The *spikes* indicate switching signs
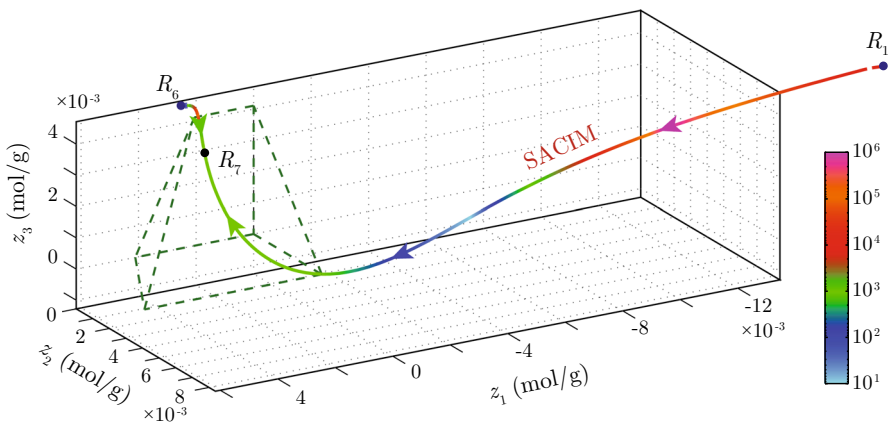
Fig. 21 The SACIMs for the simple hydrogen–oxygen system are *colored* based on the relative slowness κ. The *solid dots* are finite critical points; R_7 represents the system's physical equilibrium state, R_1 and R_6 represent the starting points of the SACIMs, and the *dashed simplex* represents the physical domain (Color figure online)

4 Conclusions

Diagnostic techniques based on local linearization near a manifold are seen to have value in answering the question posed by Lorenz [10]: "the slow manifold–what is it?" More particularly, these diagnostic tools can be applied to any candidate manifold, including a CIM, and answer whether or not the manifold is both slow and attractive in the neighborhood of the CIM. A related question which is as important in practical applications—the slow manifold–where is it?–remains unanswered. The CIM identified by heteroclinic connection of saddle and sink equilibria is clearly a viable candidate, but we have shown by example with a simplified three-dimensional model problem that even for a CIM on which a local volume element is shrinking, the rotation of that same element may not be sufficiently rapid to overcome localized growth away from the CIM. Thus, any reduction algorithm which relies on projection onto such a CIM in regions far from equilibrium would likely induce significant error in

the prediction of many state variables. For two problems, each built on an actual combustion model, we in fact identified SACIMs. It remains to be seen whether all such CIMs are SACIMs. In the absence of a constructive method guaranteed to identify a SACIM, it is should be considered that any manifold intended for use in a combustion chemistry problem be subjected to diagnostics based on local linearization over the span of expected conditions. It is recognized that this would be a daunting task for practical combustion problems. In addition, the tools developed here based on local analysis near the CIM cannot speak to the global stability of the CIM, which remains an even more challenging problem.

References

1. C.K. Law, *Combustion Physics* (Cambridge University Press, New York, 2006)
2. J.D. Mengers, J.M. Powers, SIAM J. Appl. Dyn. Syst. **12**(2), 560–595 (2013)
3. J.D. Mengers, Slow Invariant Manifolds for Reaction–Diffusion Systems (Ph.D. Dissertation, University of Notre Dame, 2012)
4. S.H. Lam, D.A. Goussis, Symp. Int. Combust. Proc. **22**(1), 931–941 (1989)
5. U. Maas, S.B. Pope, Combust. Flame **88**(3–4), 239–264 (1992)
6. M.R. Roussel, J. Math. Chem. **21**(4), 385–393 (1997)
7. A. Büki, T. Perger, T. Turśnyi, U. Maas, J. Math. Chem. **31**(4), 345–362 (2002)
8. E.N. Lorenz, J. Atmos. Sci. **43**(15), 1547–1557 (1986)
9. E.N. Lorenz, V. Krishnamurthy, J. Atmos. Sci. **44**(20), 2940–2950 (1987)
10. E.N. Lorenz, J. Atmos. Sci. **49**(24), 2449–2451 (1992)
11. R. Camassa, S.-K. Tin, J. Atmos. Sci. **53**(22), 3251–3264 (1996)
12. J.-M. Ginoux, Qual. Theory Dyn. Syst. **13**(1), 19–37 (2014)
13. K. Nipp, D. Stoffer, *Invariant Manifolds in Discrete and Continuous Dynamical Systems* (European Mathematical Society, Zürich, 2013)
14. A. Adrover, F. Creta, M. Giona, M. Valorani, J. Comput. Phys. **225**(2), 1442–1471 (2007)
15. M.J. Davis, R.T. Skodje, J. Chem. Phys. **111**(3), 859–874 (1999)
16. J.M. Powers, S. Paolucci, Am. J. Phys. **76**(9), 848–855 (2008)
17. L. Perko, *Differential Equations and Dynamical Systems* (Springer, Berlin, 2001)
18. R. Aris, *Vectors, Tensors and the Basic Equations of Fluid Mechanics* (Dover, New York, 1989)
19. J.-M. Ginoux, B. Rossetto, Int. J. Bifurcat. Chaos **16**(4), 887–910 (2006)
20. M.R. Roussel, S.J. Fraser, J. Phys. Chem. **97**(31), 8316–8327 (1993)
21. Z. Ren, S.B. Pope, Combust. Theor. Model. **10**(3), 361–388 (2006)
22. A.N. Al-Khateeb, J.M. Powers, S. Paolucci, A.J. Sommese, J.A. Diller, J.D. Hauenstein, J.D. Mengers, J. Chem. Phys. **131**(2), 024118 (2009)
23. Z. Ren, S.B. Pope, A. Vladimirsky, J.M. Guckenheimer, J. Chem. Phys. **124**(11), 114111 (2006)
24. D.J. Higham, L.N. Trefethen, Bit **33**(2), 285–303 (1993)
25. L.N. Trefethen, M. Embree, *Spectra and Pseudospectra: The Behavior of Nonnormal Matrices and Operators* (Princeton University Press, Princeton, 2005)